Merger shocks enhance quenching in local galaxy clusters

Roberts, I.D.

The Astrophysical Journal, 971:182 (5pp), 2024 August 20 https://doi.org/10.3847/1538-4357/ad67d0

Merger Shocks Enhance Quenching in Local Galaxy Clusters

Ian D. Roberts[1,2,3]
[1] Department of Physics & Astronomy, University of Waterloo, Waterloo, ON N2L 3G1, Canada; ianr@uwaterloo.ca
[2] Waterloo Centre for Astrophysics, University of Waterloo, 200 University Ave. W, Waterloo, ON N2L 3G1, Canada
[3] Leiden Observatory, Leiden University, PO Box 9513, 2300 RA Leiden, The Netherlands
Received 2024 July 8; revised 2024 July 22; accepted 2024 July 24; published 2024 August 20

Abstract

We report evidence for enhanced quenching in low-redshift galaxy clusters hosting radio relics. This effect is strongest for low-mass galaxies and is consistent with a rapid quenching of star formation. These results imply that merger shocks in the intracluster medium play a role in driving environmental quenching, which we argue is due to elevated ram pressure in these disturbed systems.

Unified Astronomy Thesaurus concepts: Galaxy clusters (584); Galaxy evolution (594); Star formation (1569); Galaxy quenching (2040); Radio continuum emission (1340)

1. Introduction

Galaxy clusters are the most massive gravitationally bound objects in the Universe. The primary channel for the mass growth of clusters is hierarchical merging, both via accretion of lower mass groups, as well as major mergers with similar-mass clusters. Major cluster mergers are among the most energetic events in the Universe, capable of releasing energies of 10^{64} erg or more (e.g., Sarazin 2002). Mergers deposit new galaxies as well as drive shocks, increased turbulence, and sloshing motions through the intracluster medium (ICM). These effects can be observed through galaxy substructure and non-Gaussian velocity distributions (e.g., Yahil & Vidal 1977; Dressler & Shectman 1988; Hou et al. 2009; Martínez & Zandivarez 2012), asymmetric X-ray distributions (e.g., Rasia et al. 2013; Weißmann et al. 2013), and diffuse radio continuum emission in the form of radio relics and halos (e.g., Feretti et al. 2012; van Weeren et al. 2019).

Given the increased velocity dispersions and ICM motions in disturbed systems, cluster mergers may be expected to impact the evolution of member galaxies. In particular, the dependence of ram pressure stripping on the relative velocity between galaxies and the ICM (e.g., Gunn & Gott 1972) implies that all else equal, dynamical disturbances will increase the strength of ram pressure. Results on the effect of cluster dynamical state on galaxy evolution are mixed, with some studies finding an excess of star-forming galaxies in merging/disturbed clusters (e.g., Ribeiro et al. 2010; Carollo et al. 2013; Stroe et al. 2015; Roberts & Parker 2017; Stroe et al. 2017) and others finding a deficit (e.g., Pranger et al. 2014; Deshev et al. 2017). Many (though not all) of these previous studies are based on classifications according to the group/cluster velocity distribution (i.e., Gaussian or non-Gaussian); however, such classifications can be highly uncertain due to projection effects (Roberts & Parker 2019).

A far more reliable tracer of recent merger history is the presence of a radio relic.[4] Radio relics are diffuse synchrotron-emitting structures observed in the radio continuum. It is broadly accepted that these relics trace shock fronts from cluster mergers, in which cosmic-ray electrons are accelerated by diffusive shock acceleration (e.g., Blandford & Ostriker 1978; Jones & Ellison 1991; Malkov & Drury 2001). Therefore, observing relics in clusters provides an avenue to generate samples of merging clusters with high purity.

In this paper, we compile all clusters in the Sloan Digital Sky Survey (SDSS) at low redshift with known radio relics. The purpose of this work is to address one simple, but important, question: does the presence of a merger shock impact star formation quenching in low-redshift clusters? As outlined above, constraints on this question will provide insight into the physical mechanisms driving environmental quenching in clusters.

The outline of this paper is as follows. In Section 2 we describe our cluster and galaxy samples, in Section 3 we present observed quenched fractions for galaxies in clusters hosting a radio relic (relative to a control sample), and in Section 4 we provide a discussion and conclusions. Throughout, we assume a flat ΛCDM cosmology with $H_0 = 70\,\mathrm{km\,s^{-1}\,Mpc^{-1}}$, $\Omega_M = 0.3$, and $\Omega_\Lambda = 0.7$.

2. Data and Methods

2.1. Cluster Sample

We select all galaxy clusters at $z < 0.1$ with known radio relics. Clusters hosting radio relics are drawn from van Weeren et al. (2019) and Botteon et al. (2022). From these compilations, we select all clusters at $z < 0.1$ that are classified as hosting either a confirmed or a candidate radio relic. Only one cluster in our sample, A2255, is classified as a candidate radio relic (van Weeren et al. 2019). We also require that the clusters are within the footprint of the main SDSS spectroscopic sample. This gives nine clusters that form our radio relic sample listed in Table 1.

For comparison, we also define a control sample of galaxy clusters drawn from the Yang et al. (2007) SDSS group catalog. We restrict to clusters that fall within the redshift and halo mass range of our radio relic sample ($z < 0.1$ and $14.4 \leqslant \log\,[M_h/M_\odot] \leqslant 15.0$). After removing the systems that make up our radio relic sample, this leaves 121 control clusters. Given the relative rarity of relics in clusters (e.g., Botteon et al. 2022), it is almost certain that this control sample is dominated

[4] For the remainder of the paper, when referring to radio relics we are specifically referring to the *radio gischt* class that is associated with merger shocks.

Table 1
Clusters Hosting a Radio Relic

Name	Y07 ID[a]	Redshift[b]	R.A.[b]	Decl.[b]	$\log(M_h/M_\odot)$[c]	N_{gal}[d]
Abell 1367	3	0.0225	11h44m44.60 s	+19d41m59.0 s	14.6	168
Abell 1656	1	0.0234	12h59m44.40 s	+27d54m44.9 s	14.9	700
Abell 0168	25	0.0451	01h15m07.58 s	+00d19m10.8 s	14.5	172
Abell 1904	26	0.0718	14h22m13.21 s	+48d35m59.7 s	14.8	156
RXCJ1053.7 + 5452	146	0.0720	10h53m50.83 s	+54d49m55.1 s	14.4	55
Abell 2061	29	0.0783	15h21m19.90 s	+30d37m13.0 s	14.9	166
Abell 2255	32	0.0801	17h12m50.04 s	+64d03m10.6 s	15.0	231
Abell 2249	218	0.0849	17h09m36.76 s	+34d28m04.1 s	14.5	109
Abell 0610	277	0.0970	07h59m21.77 s	+27d08m29.2 s	14.4	44

Notes.
[a] modelC_group catalog from Yang et al. (2007).
[b] SIMBAD database (https://simbad.unistra.fr/simbad/).
[c] Abundance matching from Yang et al. (2007).
[d] Spectroscopic member galaxies according to criteria in Section 2.2.

by clusters that do not host a radio relic, though this has not been explicitly confirmed (and the requisite data do not exist to do so for all clusters in the control sample).

2.2. Galaxy Sample

We select member galaxies for each of our clusters based on offsets in projected radius and velocity from the cluster center. We consider galaxies to be members of a given cluster if they are within R_{180} and have a velocity offset of less than 3000 km s^{-1}. The qualitative results are unchanged if instead we use a velocity offset of $<3\sigma_v$. We follow Yang et al. (2007) and calculate R_{180} as

$$R_{180} = 1.26\,h^{-1}\,\mathrm{Mpc}\left(\frac{M_h}{10^{14}\,h^{-1}\,M_\odot}\right)^{1/3}(1+z_{\mathrm{clust}})^{-1}, \quad (1)$$

where z_{clust} is the cluster redshift. Lastly, we only select galaxies with $\log(M_\star/M_\odot) \geqslant 9.5$. The parent catalog from which galaxies are selected is the GALEX-SDSS-WISE Legacy Catalog (GSWLC; Salim et al. 2016, 2018). We also take stellar masses and star formation rate estimates for each member galaxy from the GSWLC.

The median galaxy redshifts for the radio relic and control galaxy samples are 0.05 and 0.07, respectively, which correspond to an SDSS stellar mass completeness of $\log(M_\star/M_\odot) \simeq 10$ (Weigel et al. 2016). Thus, we are not stellar mass complete over our full mass range; however, both the radio relic and control samples have similar redshift distributions and thus should be similarly incomplete. We note that we also compute quenched fractions in narrow bins of stellar mass in order to further mitigate any stellar mass dependencies.

While the radio relic and control clusters span the same range in halo mass, the relic-hosting clusters are skewed toward larger halo mass than the control (see Figure 1, top). As quenched fractions correlate with host halo mass (e.g., Wetzel et al. 2012), we take two different approaches to ensure that this halo-mass bias is not driving the results presented in this work.

Our first approach is to reweight the galaxies in each sample in order to ensure a fair comparison. Weights are derived in narrow bins of halo mass:

$$\log(M_h/M_\odot) = [14.4, 14.6),\ [14.6, 14.8),\ [14.8, 15.0),\ [15.0, 15.2). \quad (2)$$

For each halo mass bin, i, the weight is calculated as

$$w_i = \frac{N_{\mathrm{total}}}{N_i}, \quad (3)$$

where N_{total} is the total number of galaxies for a given sample and N_i is the number of galaxies for that sample that fall within the halo mass bin, i. Weights are calculated separately for the control and radio relic galaxy samples, and when applied have the effect of enforcing a roughly uniform halo mass distribution over our sample range (see Figure 1, middle). We also experimented with different weighting schemes, as well as applying no weighting at all. In no cases did these variations affect the scientific conclusions from this work.

Our second approach is to construct a smaller control sample that is matched to the halo mass distribution for the radio relic sample. In the same halo mass bins as used for the weighting, for each galaxy in the radio relic sample we randomly draw a galaxy from the control sample within the same halo mass bin. This gives a control sample that is of equal size and matched in halo mass to the relic sample. When doing computations with the matched control sample, we always take the median of 1000 random realizations of the matched control sample in order to account for the random nature of the matching procedure.

In Figure 1 (middle and bottom) we show the halo mass distributions resulting from the sample weighting and the sample matching described above. In both cases, the result is a control sample that is well-matched to the halo mass distribution of the radio relic sample.

2.3. Quenched Fractions

In general, the quenched fraction for a given set of galaxies is calculated as

$$f_Q = \frac{N_{\mathrm{Q}}}{N}, \quad (4)$$

where N_{Q} and N are the number of quenched galaxies and the total number of galaxies, respectively. To identify quenched

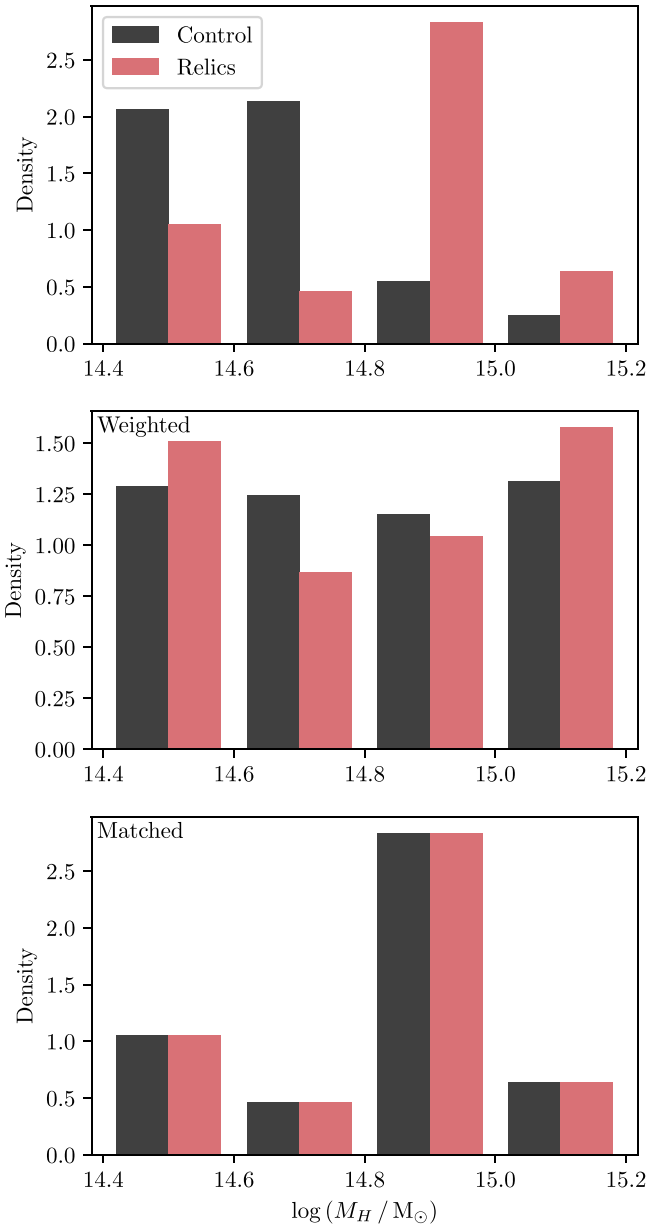

Figure 1. Distributions of host halo mass for galaxies in the radio relic (red) and control (black) samples. The top panel shows the unweighted distributions. The middle panel shows distributions where galaxies are weighted in order to match the halo mass distributions for the two samples (see Equation (3)). The bottom panel shows distributions for the radio relic sample and a subset of the control sample that is matched according to halo mass.

galaxies we follow numerous previous works (e.g., Wetzel et al. 2012) and use a single cut in specific star formation rate (sSFR = SFR/$M_\star$) at $\log(\mathrm{sSFR}/\mathrm{yr}^{-1}) = -11$.

We calculate quenched fractions in narrow bins of stellar mass. When comparing the radio relic and matched control samples we compute quenched fractions according to Equation (4). We also apply the weights described in Section 2.2, and in this case, the weighted quenched fraction is given by

$$f_Q = \frac{\sum w(\log \mathrm{sSFR} < -11)}{\sum w}. \quad (5)$$

3. Results

In Figure 2 we show the main scientific result of this paper, galaxies within clusters with radio relics have enhanced quenched fractions relative to the control cluster sample. This enhancement is most clear at the low-mass end, consistent with many previous works showing that environmental quenching effects preferentially impact low-mass galaxies (at least at low-z; e.g., Haines et al. 2006; Bamford et al. 2009; Peng et al. 2010; Roberts et al. 2019). In the lowest-mass bins, the quenched fraction in the radio relic sample is at least a factor of 2 above the control. These statements hold regardless of whether we consider the weighted samples (left) or the matched control sample (right).

For low-mass galaxies ($9.5 \leqslant \log[M_\star/M_\odot] < 10.5$), the quenched fraction shows a 6σ and 12σ excess relative to the control sample, for the weighted and matched samples, respectively. For the case of the matched approach, we measure the excess relative to the median of the random matches. Conservatively, we conclude that galaxies in the radio relic sample have enhanced quenched fractions at greater than 6σ significance. For high-mass galaxies ($10.5 \leqslant \log[M_\star/M_\odot] < 11.5$), this excess is weaker in magnitude and at lesser significance (2σ–4σ).

In Figure 3 we show the sSFR distributions for the relic and control samples, including a double-Gaussian fit for each sample. The distributions in Figure 3 are weighted according to Equation (3), though we note that the same conclusions hold when instead considering the matched control and unweighted relic samples. This again shows the excess of quenched galaxies in the radio relic clusters. The shape of the high-sSFR Gaussian component, corresponding to the star-forming population, is nearly identical for the control and radio relic samples (modulo normalization). This is consistent with the difference between the two samples being driven by a rapid quenching process where the quenching timescale is short relative to the gas depletion timescale (see, e.g., Wetzel et al. 2012).

4. Discussion and Conclusions

The excess in quenched galaxies for clusters with radio relics has important implications for the physical drivers of environmental quenching. The efficiency with which galaxies are quenched appears to be enhanced in the presence of merger-induced motions and shock waves in the ICM. The most commonly invoked mechanisms for explaining environmental quenching in low-z clusters are the ram pressure stripping of cold gas and starvation (see Cortese et al. 2021; Boselli et al. 2022 for recent reviews). Starvation is sometimes subdivided into gas consumption associated with the stripping of the circumgalactic medium (CGM), versus gas consumption in association with the inability of new gas to cool and condense out of the CGM due to the high virial temperature of the cluster. The former is simply a manifestation of a moderate ram pressure whereas the latter is more physically distinct.

Because ram pressure has a quadratic dependence on the relative velocity between the galaxy and the ICM, the strength of ram pressure should be enhanced (all else equal) in the presence of sloshing motions, and especially in the vicinity of shocks moving through the ICM. Thus, the excess quenched fraction shown in Figure 2 favors a ram pressure-like quenching mechanism, with the cold interstellar medium

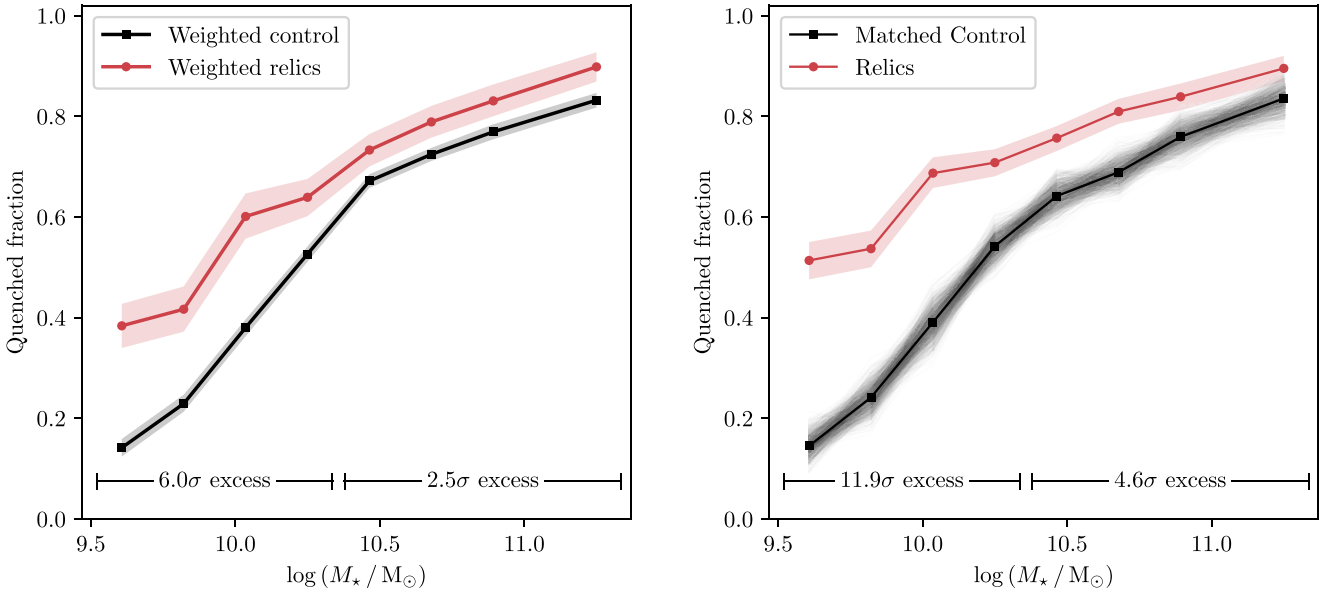

Figure 2. Left: weighted quenched fraction as a function of stellar mass for galaxies in the radio relic (red) and control (black) samples. The vertical shading corresponds to the 16 and 84 percentile confidence interval on the quenched fraction, derived via bootstrap resampling. Right: quenched fraction as a function of stellar mass for galaxies in the radio relic (red) and matched control (black) samples. For the relic sample, the vertical shading again corresponds to the 16 and 84 percentile bootstrap confidence interval on the quenched fraction. For the matched control sample, the faded lines correspond to the individual trends for each random realization of the matching procedure (see the main text for details), and the heavier line type marks the median of these realizations.

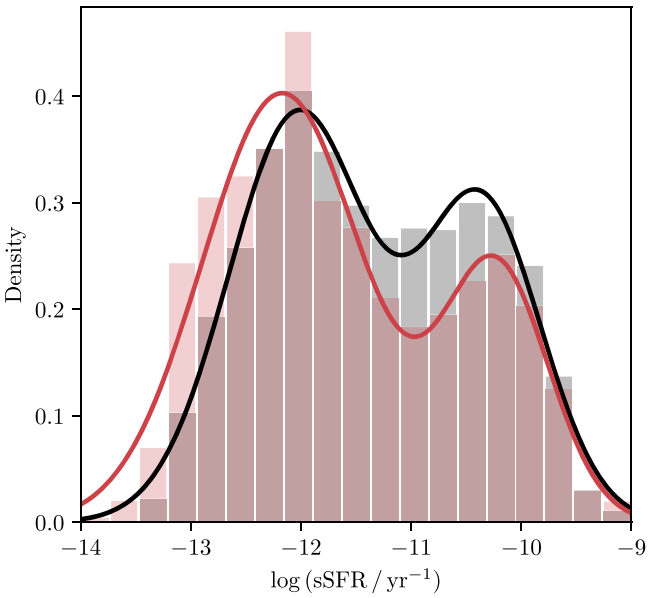

Figure 3. Specific star formation rate distributions for the control and radio relic samples. Both distributions have been weighted according to Equation (3). Observed distributions are shown by histograms and we also overlay the best-fit double-Gaussian distribution for each each sample.

and/or the CGM being removed, as opposed to a starvation scenario tied to the lack of gas cooling.

This is not the first time that quenching, particularly via ram pressure stripping, has been associated with diffuse radio relics in clusters. The best-known example would be Abell 1367 (a member of our radio relic cluster sample), where three prominent jellyfish galaxies are spatially coincident with the radio relic to the northwest of the cluster center (Gavazzi & Jaffe 1987; Gavazzi et al. 2001; Roberts et al. 2021). It is both thought that the merger shock has contributed to the extreme stripped tails observed for these galaxies and that the radio continuum tails in turn feed the radio relic with seed cosmic-ray electrons (Ge et al. 2019). Unfortunately, the number of known jellyfish galaxies in clusters hosting radio relics is small (likely $\lesssim$50), leaving any attempted association between relics and stripped tails with extremely limited statistical power.

At intermediate redshift, Stroe et al. (2015, 2017) show that merging clusters (as traced by radio haloes and/or relics) host an excess of Hα emitters relative to relaxed clusters (and the field). This is attributed to gas compression from ICM shocks catalyzing star formation and is consistent with works at low redshift finding enhanced star formation rates in galaxies experiencing ram pressure stripping (e.g., Gavazzi et al. 2001; Vulcani et al. 2018; Roberts & Parker 2020; Roberts et al. 2022). At similar redshifts, Ebeling et al. (2014), Ebeling & Kalita (2019), and McPartland et al. (2016) find a number of jellyfish galaxies with tails of extra-planar material, which they argue are preferentially associated with ongoing cluster mergers. This rapid gas consumption, in concert with gas removal via increased ram pressure, may lead to rapid quenching and thus the excess of quenched galaxies that we observe at $z \sim 0$.

This work clearly shows excess environmental quenching associated with the presence of ICM shocks. With more radio relic detections moving forward, for example with the completion of the LOFAR Two-meter Sky Survey (Shimwell et al. 2017, 2019, 2022) as well as future surveys from the Square Kilometre Array, these conclusions can be strengthened further. An ultimate goal will be to directly test whether ram pressure-tailed galaxies are associated with the location (and path) of merger shocks in clusters.

Acknowledgments

We thank Laura Parker and Mike Hudson for giving feedback on an early draft. I.D.R. acknowledges support from the Banting Fellowship Program.

Facility: Sloan.

Software: AstroPy (Astropy Collaboration et al. 2013), Matplotlib (Hunter 2007), NumPy (Harris et al. 2020).

ORCID iDs

Ian D. Roberts https://orcid.org/0000-0002-0692-0911

References

Astropy Collaboration, Robitaille, T. P., Tollerud, E. J., et al. 2013, A&A, 558, A33
Bamford, S. P., Nichol, R. C., Baldry, I. K., et al. 2009, MNRAS, 393, 1324
Blandford, R. D., & Ostriker, J. P. 1978, ApJL, 221, L29
Boselli, A., Fossati, M., & Sun, M. 2022, A&AR, 30, 3
Botteon, A., Shimwell, T. W., Cassano, R., et al. 2022, A&A, 660, A78
Carollo, C. M., Cibinel, A., Lilly, S. J., et al. 2013, ApJ, 776, 71
Cortese, L., Catinella, B., & Smith, R. 2021, PASA, 38, e035
Deshev, B., Finoguenov, A., Verdugo, M., et al. 2017, A&A, 607, A131
Dressler, A., & Shectman, S. A. 1988, AJ, 95, 985
Ebeling, H., & Kalita, B. S. 2019, ApJ, 882, 127
Ebeling, H., Stephenson, L. N., & Edge, A. C. 2014, ApJL, 781, L40
Feretti, L., Giovannini, G., Govoni, F., & Murgia, M. 2012, A&ARv, 20, 54
Gavazzi, G., Boselli, A., Mayer, L., et al. 2001, ApJL, 563, L23
Gavazzi, G., & Jaffe, W. 1987, A&A, 186, L1
Ge, C., Sun, M., Liu, R.-Y., et al. 2019, MNRAS, 486, L36
Gunn, J. E., & Gott, J. R., III 1972, ApJ, 176, 1
Haines, C. P., La Barbera, F., Mercurio, A., Merluzzi, P., & Busarello, G. 2006, ApJL, 647, L21
Harris, C. R., Millman, K. J., van der Walt, S. J., et al. 2020, Natur, 585, 357
Hou, A., Parker, L. C., Harris, W. E., & Wilman, D. J. 2009, ApJ, 702, 1199
Hunter, J. D. 2007, CSE, 9, 90
Jones, F. C., & Ellison, D. C. 1991, SSRv, 58, 259
Malkov, M. A., & Drury, L. O. 2001, RPPh, 64, 429
Martínez, H. J., & Zandivarez, A. 2012, MNRAS, 419, L24
McPartland, C., Ebeling, H., Roediger, E., & Blumenthal, K. 2016, MNRAS, 455, 2994
Peng, Y.-j., Lilly, S. J., Kovač, K., et al. 2010, ApJ, 721, 193
Pranger, F., Böhm, A., Ferrari, C., et al. 2014, A&A, 570, A40
Rasia, E., Meneghetti, M., & Ettori, S. 2013, AstRv, 8, 40
Ribeiro, A. L. B., Lopes, P. A. A., & Trevisan, M. 2010, MNRAS, 409, L124
Roberts, I. D., Lang, M., Trotsenko, D., et al. 2022, ApJ, 941, 77
Roberts, I. D., & Parker, L. C. 2017, MNRAS, 467, 3268
Roberts, I. D., & Parker, L. C. 2019, MNRAS, 490, 773
Roberts, I. D., & Parker, L. C. 2020, MNRAS, 495, 554
Roberts, I. D., Parker, L. C., Brown, T., et al. 2019, ApJ, 873, 42
Roberts, I. D., van Weeren, R. J., McGee, S. L., et al. 2021, A&A, 650, A111
Salim, S., Boquien, M., & Lee, J. C. 2018, ApJ, 859, 11
Salim, S., Lee, J. C., Janowiecki, S., et al. 2016, ApJS, 227, 2
Sarazin, C. L. 2002, in Merging Processes in Galaxy Clusters, ed. L. Feretti, I. M. Gioia, & G. Giovannini (Berlin: Springer), 1
Shimwell, T. W., Hardcastle, M. J., Tasse, C., et al. 2022, A&A, 659, A1
Shimwell, T. W., Röttgering, H. J. A., Best, P. N., et al. 2017, A&A, 598, A104
Shimwell, T. W., Tasse, C., Hardcastle, M. J., et al. 2019, A&A, 622, A1
Stroe, A., Sobral, D., Dawson, W., et al. 2015, MNRAS, 450, 646
Stroe, A., Sobral, D., Paulino-Afonso, A., et al. 2017, MNRAS, 465, 2916
van Weeren, R. J., de Gasperin, F., Akamatsu, H., et al. 2019, SSRv, 215, 16
Vulcani, B., Poggianti, B. M., Gullieuszik, M., et al. 2018, ApJL, 866, L25
Weigel, A. K., Schawinski, K., & Bruderer, C. 2016, MNRAS, 459, 2150
Weißmann, A., Böhringer, H., Šuhada, R., & Ameglio, S. 2013, A&A, 549, A19
Wetzel, A. R., Tinker, J. L., & Conroy, C. 2012, MNRAS, 424, 232
Yahil, A., & Vidal, N. V. 1977, ApJ, 214, 347
Yang, X., Mo, H. J., van den Bosch, F. C., et al. 2007, ApJ, 671, 153